
How Much of a Model Do We Need? Redundancy and Slimmability in Remote Sensing Foundation Models

Leonard Hackel^{1,2} Tom Burgert^{1,2} Begüm Demir^{1,2}

Abstract

Large-scale foundation models (FMs) in remote sensing (RS) are developed based on the paradigms established in computer vision (CV) and have shown promise for various Earth observation applications. However, the direct transfer of scaling assumptions from CV to RS has not been adequately examined. We hypothesize that RS FMs enter an overparameterized regime at substantially smaller scales than their CV counterparts, where increasing parameter count primarily induces redundant representations rather than qualitatively new abstractions. To test this hypothesis, we use post-hoc slimming, where we uniformly reduce the width of pretrained encoder, as a tool to measure representational redundancy across six state-of-the-art RS FMs on four downstream classification tasks. Our findings reveal a significant contrast with those in the CV domain: while a post-hoc slimmed masked autoencoder (MAE) trained on ImageNet retains less than 10 % accuracy at 1 % FLOPs, RS FMs maintain over 71 % relative accuracy at the same budget. This sevenfold difference provides strong empirical support for our hypothesis. We further demonstrate that learned slimmable training can improve both Momentum Contrast (MoCo)- and MAE-based models. In addition, through the explained variance ratio and the feature correlation analysis, we provide mechanistic explanations showing that RS FMs distribute task-relevant information with high redundancy. Our findings establish post-hoc slimmability as both a practical deployment strategy for resource-constrained environments and a diagnostic tool that challenges the prevailing scaling paradigm in RS. Upon acceptance, we will publish all code.

¹Big Data Analytics for Earth Observation, Berlin Institute for the Foundations of Learning and Data, Berlin, Germany

²remote sensing (RS) Image Analysis Group, Technische Universität Berlin, Berlin, Germany. Correspondence to: Leonard Hackel <l.hackel@tu-berlin.de>.

Preprint. February 2, 2026.

1. Introduction

Remote sensing (RS) images acquired by satellite or airborne systems are a rich source of information to monitor the Earth surface, e.g., for climate change analysis, urban area studies, risk and damage assessment, and crop monitoring (Yang et al., 2013; Maktav et al., 2005; Yamazaki & Matsuoka, 2007; Omia et al., 2023). With the rapid emergence of large-scale RS foundation models (FMs) trained on extensive image archives, practitioners have shifted from training single-purpose models to finetuning pretrained FMs (Jiao et al., 2023; Xiao et al., 2025; Lu et al., 2025). Many of these FMs explicitly follow the paradigms established in computer vision (CV), most notably self-supervised learning (SSL) paradigms such as contrastive learning or masked image modeling (MIM), as well as multimodal pretraining strategies inspired by DINO (Zhang et al., 2023) and CLIP (Radford et al., 2021) in CV. In line with prevailing practices in CV, these RS FMs are typically scaled by increasing parameter count, often with the implicit assumption that larger models yield more universal and transferable representations. However, the direct transfer of scaling assumptions from CV to RS remains insufficiently examined. While both domains rely on visual data, they differ substantially in data characteristics such as spatial and spectral resolution. Recent analyses indicate that models trained on RS data depend predominantly on low- and mid-level features, whereas models trained on natural images exhibit stronger reliance on higher-level semantic abstractions (Burgert et al., 2025). These differences raise a fundamental question: Do the benefits of model scaling observed in CV FMs translate equally to RS, or do they induce qualitatively different representational regimes?

Building on these observations, we hypothesize that RS FMs enter an overparameterized regime at substantially smaller scales than their CV counterparts. Beyond this point, increasing parameter count primarily induces redundant representations of task-relevant features rather than qualitatively new abstractions, distributing task-relevant information across many interchangeable parameters rather than encoding it sparsely (Doimo et al., 2022). This creates an ‘implicit ensemble’ where marginal performance gains from scaling arise from averaging redundant features

rather than learning fundamentally better ones. This hypothesis yields a clear prediction: If RS FMs rely on highly redundant representations, even unstructured, task-agnostic parameter removal should preserve substantial downstream performance. Conversely, if task-relevant information were sparsely encoded, parameter removal would require structured or task-aware pruning to retain performance. We therefore use uniform width reduction of the pretrained encoder transformer blocks, which we call post-hoc slimmability, as a tool to measure representational redundancy. Moreover, if overparameterization in RS FMs is systematic, explicitly incorporating slimmability during training provides a means to examine whether this redundancy can be structured more consistently.

To test these hypotheses, we conduct a comprehensive empirical study across six state-of-the-art RS FMs ranging from 86 M to 631 M parameters, pretrained on datasets of 4 M–11 M images with compute budgets spanning 100 to 58 000 GPU-hours. We evaluate slimmability on four downstream classification tasks using frozen feature extraction with k-nearest neighbors (k-NN) classifiers, examining performance retention across computational budgets from 1 % to 100 % of full model capacity. As shown in Figure 1, our findings reveal a significant contrast with those in the CV domain: while a post-hoc slimmed masked autoencoder (MAE) trained on ImageNet retains less than 10 % relative accuracy at 1 % floating-point operations (FLOPs) when evaluated on ImageNet-100 (Tian et al., 2020), RS FMs maintain more than 71 % relative accuracy at the same computational budget across all evaluated models and tasks. This sevenfold difference provides strong empirical support for our hypothesis that RS FMs operate in a fundamentally different representational regime than their CV counterparts.

Beyond its explanatory role, slimmability has direct practical relevance in RS. Deploying or finetuning large FMs is often infeasible due to restricted data access, licensing constraints, and substantial computational requirements. Post-hoc slimmability provides a mechanism for adapting pretrained models to available resources without access to original training data or large-scale compute. This need is amplified by operational variability: inference requirements change substantially depending on spatial extent or temporal frequency (e.g., local analysis vs continuous large-area monitoring), while deployment settings include on-board satellite systems with strict memory, power, and latency constraints where a single fixed-capacity FM cannot accommodate such tightly constrained operating conditions.

Our main contributions are as follows:

- (1) We present the first systematic study of slimmability in

²The MAE baseline is https://huggingface.co/timm/vit_base_patch16_224.mae.

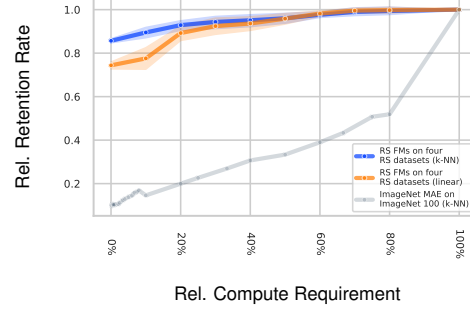


Figure 1. Averaged relative retention rate of six RS FMs across four datasets with respect to their computational budget when slimmed post-hoc in comparison with a CV MAE baseline. RS FMs retain over 70 % relative accuracy at all slimming scales for both k-NN and linear probing, whereas a MAE trained on ImageNet-1k (Russakovsky et al., 2015) and evaluated on ImageNet-100 (Tian et al., 2020) exhibits sharp degradation.²

RS FMs, demonstrating that existing RS FMs can be slimmed post-hoc with surprisingly small performance degradation. This contrasts with the CV domain and establishes post-hoc slimmability as a practical tool for resource-constrained practitioners.

- (2) We provide an empirical comparison between post-hoc and learned slimmability through controlled experiments with Momentum Contrast (MoCo) and MAE, showing that learned slimmable training can outperform post-hoc slimming in accuracy and robustness across slimming ratios, establishing learned slimmability as a desirable property for future RS FMs.
- (3) We conduct an in-depth analysis of model properties governing slimmability through explained variance and feature correlation analysis, revealing how training paradigms and architectural components affect slimming robustness and providing mechanistic explanations for the observed differences between different FMs.

2. Related Work

Slimmable Networks and Model Compression. Slimmable neural networks enable a single model to operate at multiple widths, facilitating dynamic accuracy-efficiency trade-offs at runtime. We distinguish two paradigms: i) *post-hoc slimmability*, where uniform width reduction is applied to pretrained models; and ii) *learned slimmability*, where models are trained with explicit width sampling from scratch. (Yu et al., 2019) pioneer the second paradigm by introducing switchable batch normalization (BN), which maintains independent BN parameters for each width, achieving competitive ImageNet accuracy through joint training. (Yu & Huang, 2019) extend this with Universally Slimmable Networks (US-Nets), which generalize to

arbitrary widths via post-statistics BN recalibration and the sandwich rule for width sampling during training. (Li et al., 2021) introduce Dynamic Slimmable Networks (DS-Net) with adaptive gates for test-time width selection, achieving $2\text{--}4\times$ computation reduction on ImageNet.

Extending slimmability to SSL introduces challenges due to the interaction between multi-width optimization and representation learning. (Cao et al., 2023) demonstrate that naive SSL application to slimmable networks causes training collapse. To address this issue, they present US3L which implements temporally consistent guidance and dynamic width sampling. (Zhao et al., 2025) introduce SlimCLR with slow-start training that optimizes full-width models before progressively introducing narrower sub-networks. However, these works focus exclusively on contrastive methods in CV, leaving slimmable MAE approaches and applications to RS FMs unexplored.

Alternative compression techniques include structured pruning (Li et al., 2017; Liu et al., 2017), which removes channels based on importance scores, knowledge distillation (Hinton et al., 2015), which transfers knowledge through soft targets, and quantization (Jacob et al., 2018), which reduces numerical precision. However, these methods typically require access to training data for retraining, task-specific optimization, or specialized hardware. In contrast, slimmable networks enable dynamic width adjustment at inference without task-specific retraining, making them suitable for scenarios with limited data access or varying deployment constraints.

Remote Sensing Foundation Models. With advances in SSL and the increasing availability of large-scale RS data, the development of FMs has gained significant attention as a way of learning general-purpose RS representations. These models leverage SSL objectives such as contrastive learning or MIM for pretraining on diverse sensors and tasks. As shown in Table 1, representative models span multiple orders of magnitude in parameters and computational budgets. For instance, Prithvi (Jakubik et al., 2023; Szwarcman et al., 2024) leverages Sentinel-2 and Landsat time-series data, while Satlas (Bastani et al., 2023) introduces 300M+ annotations for supervision. Beyond scaling, architectural innovations have focused on domain-specific adaptations. First, temporal and spectral modeling advances through SatMAE (Cong et al., 2022) with temporal-spectral encodings and ScaleMAE (Reed et al., 2023) with resolution-aware embeddings. Second, modality-agnostic designs have emerged, including DOFA (Xiong et al., 2024), which dynamically adapts to channel configurations, and TerraMind (Jakubik et al., 2025), which enables cross-modal generation. Third, multi-modal integration is addressed by RingMoE (Bi et al., 2025), which employs hierarchical mixture-of-experts (MoE) with modal-specialized experts.

More recently, efficiency considerations have motivated alternative architectural approaches. For example, RS-vHeat (Hu et al., 2025) replaces attention mechanisms with heat conduction operators to reduce complexity, while CSMoE (Hackel et al., 2025) achieves $2\times$ computational efficiency by utilizing the Soft MoE mechanisms. However, these approaches optimize for fixed efficiency-accuracy trade-offs at design time, consequently lacking the runtime adaptability needed for dynamic resource constraints. Despite this growing body of work, no prior research has investigated whether RS FMs exhibit different slimmability properties compared to CV models, nor explored the representational characteristics governing post-hoc slimmability in this domain.

3. Problem Setup and Evaluation Protocol

3.1. Slimmable Network Architecture

We investigate the slimmability of RS FMs by implementing dynamic width reduction in transformer blocks. For this investigation, we modify the feed-forward network (FFN) and multi-head self-attention (MHSA) layers to support variable computational budgets at inference time. In addition, we provide an analysis of individual layer types in the appendix in Section A.

Slimmable FFN. For a standard FFN with hidden dimension d_h , we implement a slimmable variant that operates on a reduced dimension $d'_h = \lfloor s \cdot d_h \rfloor$, where $s \in (0, 1]$ is the scaling factor. Given input $\mathbf{x} \in \mathbb{R}^d$, the forward pass becomes:

$$\mathbf{h} = \text{Act}(\mathbf{W}_1[:, d'_h, :] \mathbf{x} + \mathbf{b}_1[:, d'_h]), \quad (1)$$

$$\mathbf{y} = \mathbf{W}_2[:, :, d'_h] \mathbf{h} + \mathbf{b}_2, \quad (2)$$

where the weight matrices $\mathbf{W}_1 \in \mathbb{R}^{d_h \times d}$ and $\mathbf{W}_2 \in \mathbb{R}^{d \times d_h}$, and bias vectors $\mathbf{b}_1 \in \mathbb{R}^{d_h}$ and $\mathbf{b}_2 \in \mathbb{R}^d$ are sliced to their first d'_h rows, columns, or entries as indicated by the indexing notation. This reduces both computation ($\mathcal{O}(d \cdot d'_h)$ vs. $\mathcal{O}(d \cdot d_h)$) and parameters accessed during inference.

Slimmable MHSA. For multi-head attention with H heads and head dimension d_k , we reduce each head to dimension $d'_k = \lfloor s \cdot d_k \rfloor$ while maintaining all H heads. For head h , we extract indices $\mathcal{I}_h = [h \cdot d_k, h \cdot d_k + d'_k)$ and compute:

$$\mathbf{Q}_h = \mathbf{x} \mathbf{W}_Q[\mathcal{I}_h, :], \quad (3)$$

$$\mathbf{K}_h = \mathbf{x} \mathbf{W}_K[\mathcal{I}_h, :], \quad (4)$$

$$\mathbf{V}_h = \mathbf{x} \mathbf{W}_V[\mathcal{I}_h, :]. \quad (5)$$

This preserves the multi-head structure while reducing per-head dimension, yielding $\mathcal{O}(N^2 d'_k H)$ attention complexity versus $\mathcal{O}(N^2 d_k H)$ for sequence length N .

Post-hoc vs. Learned Slimmability. We distinguish two training paradigms: i) *Post-hoc slimmability* and ii) *learned*

Table 1. Landscape of selected RS FMs. Models evaluated in this work are highlighted in gray. “—” indicates information not publicly available. ⁺ multimodal; ^{*} multitemporal. For models with multiple variants, ranges indicate min–max values.

Model	#Pretraining Images	Compute Pretraining	Parameters	GFLOPs/forward pass
SatMAE (Cong et al., 2022)	713 k	768 h (V100)	330 M	—
ScaleMAE (Reed et al., 2023)	364 k	—	323 M	—
SSL4EO (Wang et al., 2023)	251 k ^{++*}	100 h (A100)	87 M	17.14
Satlas (Bastani et al., 2023)	50.4 M ^{++*}	—	86 M	17.12
SkySense (Guo et al., 2024)	21.5 M ⁺	24.6 kh (A100)	2.06 B	—
Prithvi-EO-1.0 (Jakubik et al., 2023)	4.2 M ⁺	846 h (A100)	86 M	16.98
Prithvi-EO-2.0 (Szwarcman et al., 2024)	4.2 M ^{++*}	21 kh – 58 kh (A100)	304 M – 631 M	59.85 – 162.18
DOFA (Xiong et al., 2024)	11.5 M ⁺	576 h (L40)	86 M – 330 M	17.47 – 60.47
TerraMind-1.0 (Jakubik et al., 2025)	9 M ⁺	9.2 kh (A100)	87 M – 305 M	17.83 – 61.73
RingMoE (Bi et al., 2025)	400 M ⁺	—	14.7 B	—
RS-vHeat (Hu et al., 2025)	450 k ⁺	—	—	—
CSMoE (Hackel et al., 2025)	1.1 M ⁺	—	271 M – 277 M	2.92 – 13.40

slimmability. Post-hoc slimmability applies uniform width reduction of pretrained encoder transformer blocks while preserving learned weight values. This requires no retraining, but may suffer from weight redundancy not optimized for variable widths. In contrast, learned slimmability trains models from scratch with slimmable layers and explicit width sampling during training, encouraging weight sharing and robustness across scales. The details of the training protocol are described in the appendix in Section B.

3.2. Evaluation Protocol

We evaluate our hypothesis on four RS classification benchmarks spanning diverse tasks: i) m-brick-kiln (single-label brick-kiln-presence classification, 2 classes); ii) m-eurosat (single-label land-use classification, 10 classes); iii) m-so2sat (single-label local climate zones, 17 classes); and iv) m-bigearthnet (multi-label scene classification, 43 classes). All datasets are taken from the geobench benchmark collection (Lacoste et al., 2023). For feature extraction and classification we follow standard practice for FM evaluation by adopting a frozen feature extraction protocol. For each model at scale s , we extract features from the penultimate layer and then train a k-NN classifier. Details and additional linear probing results are provided in the appendix in Section C and Section D, respectively. We report macro-averaged accuracy for the single-label datasets (m-brick-kiln, m-eurosat, and m-so2sat) and micro-mean average precision (mAP_μ) for the multi-label dataset (m-bigearthnet). We evaluate each model at 31 scales s ranging from 0.1 % to 100 % (see Section C.1 in the appendix for a complete list), measuring both classification performance and computational cost. For computational analysis, we report the *relative compute requirements* as the ratio of FLOPs at scale s to FLOPs at full scale, which directly re-

flects inference speedup from width reduction. To quantify performance degradation, we define the *relative retention rate* as $\text{RetentionRate}(s) = \text{metric}(s)/\text{metric}(1.0)$, measuring the fraction of full-model performance retained at scale s for a given metric (e.g., Accuracy or mAP_μ). We use relative retention rates when averaging results across datasets with different absolute performance levels.

To understand the intrinsic dimensionality and structure of learned representations, we analyze the explained variance ratio (EVR) of feature embeddings. For each model scale, we extract the features of the test set of a given dataset and perform a singular value decomposition on the mean-centered data matrix. Let $\sigma_1, \dots, \sigma_D$ denote the singular values of the features in descending order. The EVR of the i -th component is $\text{EVR}_i = \sigma_i^2 / \sum_j \sigma_j^2$, representing the fraction of total variance captured. We also compute the *effective dimensionality* as $d_{\text{eff}} = (\sum_i \sigma_i)^2 / \sum_i \sigma_i^2$, which quantifies how uniformly variance is distributed across components (Jing et al., 2022). A lower d_{eff} indicates more anisotropic representations in which the variance is concentrated in fewer dimensions. To assess the structure of the correlation between features, we compute the mean absolute correlation $|\text{corr}(\mathbf{e}_i, \mathbf{e}_j)|$ between all pairs of dimensions of the characteristic, providing complementary insights into the geometry of the representation in the appendix in Section E.

4. Experimental Results

4.1. Post-Hoc Slimmability of existing RS FMs

We evaluate the post-hoc slimmability of six state-of-the-art RS FMs across four downstream classification datasets of varying complexity. To this end, we examine how performance degrades as models are uniformly slimmed from full

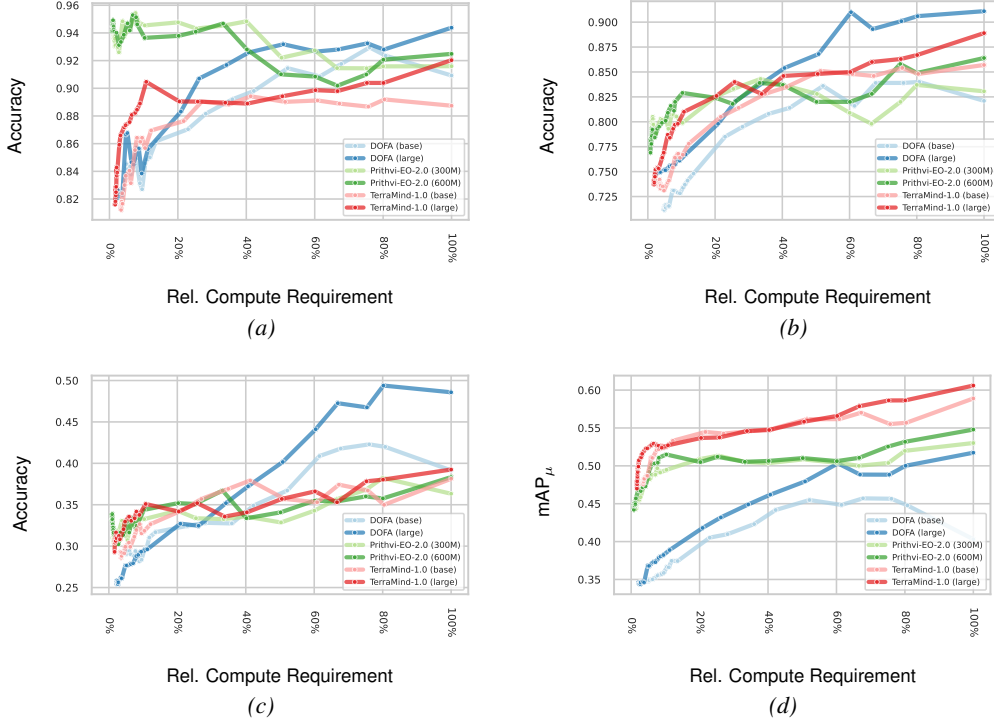


Figure 2. k-NN classification performance with respect to their relative compute requirements of six pretrained RS FMs on: a) m-brick-kiln; b) m-eurosat; c) m-so2sat; and d) m-bigearthnet from the geobench benchmark collection.

capacity ($s = 1.0$) down to 1% of computational budget. As shown in Figure 2, our results reveal that RS FMs exhibit remarkably robust post-hoc slimmability across all datasets, maintaining substantial performance even at extreme scaling. This finding contrasts sharply with those obtained using CV models, supporting our hypothesis that RS FMs operate in a fundamentally overparameterized regime.

Robust slimmability with dataset-dependent thresholds. We observe gradual degradation across all evaluated models and datasets, with performance retention and critical thresholds (where the performance drops sharply) that scale predictably with the complexity of the dataset. For the binary m-brick-kiln dataset (Figure 2a), the models retain 88–99% of the full-scale accuracy at 1% compute with no critical threshold. Instead, the accuracy degrades only gradually even below 1% compute, indicating massive redundancy in binary discriminative features. For intermediate-complexity m-eurosat (Figure 2b), all models maintain 85–95% retention at 1% compute, with gradual degradation beginning below 20% compute. The fine-grained m-so2sat dataset (Figure 2c) shows reduced but still robust retention rates of 75–86% at 1% compute, with substantial fluctuations emerging below 10% compute. For the challenging multi-label m-bigearthnet dataset (Figure 2d), models maintain 70–85% retention at 1% compute, with critical transitions between 2–10% compute. This scaling relationship demon-

strates that datasets with fewer classes require proportionally less computational budget to maintain stable performance.

Systematic non-monotonic performance peaks. Across all datasets, we observe non-monotonic behavior where intermediate scales frequently achieve higher performance than full-scale models. For m-brick-kiln, most models peak at moderate scales (7–76% compute). This behavior becomes more pronounced for intermediate-complexity datasets, with DOFA (base) peaking at 76%–81% compute on m-so2sat and m-eurosat, while TerraMind-1.0 (base) achieves effectively identical performance at 41% compute compared to full scale on m-so2sat. Even for multi-label m-bigearthnet, Prithvi-EO-2.0 (600M) achieves near-maximum performance at 8% compute with 12 \times speedup. These peaks suggest that full-scale models consistently encode redundancy that introduces noise or overfitting effects, while moderate scaling acts as implicit regularization.

Model scale and architecture effects. These results show that larger models (DOFA (large), Prithvi-EO-2.0 (600M), TerraMind-1.0 (large)) exhibit more consistent performance retention and smoother degradation curves across scales compared to their smaller counterparts. From this behavior, we can see that larger models encode dataset-relevant information more redundantly, enabling robust extraction even when heavily slimmmed. Beyond model scale, architectural

differences produce distinct slimmability profiles: DOFA’s modality-agnostic design versus Prithvi’s Sentinel-2 specialization interact with dataset requirements and model capacity to determine slimmability characteristics.

Comparison with CV models. All models across three different architectures and different model scales maintain more than 70 % relative accuracy at 1 % compute, even for the most complex dataset evaluated (m-bigearthnet). This represents an improvement over comparable CV models, where post-hoc slimming to 1 % compute yields less than 10 % retention on ImageNet-based evaluations. This significant difference strongly supports our hypothesis that RS FMs operate in a fundamentally overparameterized regime compared to their CV counterparts, with dataset-relevant information distributed redundantly across many interchangeable parameters rather than being sparsely or hierarchically encoded.

4.2. Learned vs Post-Hoc Slimmability

To investigate whether explicit slimmable training can improve upon post-hoc slimmability, we conduct controlled experiments training ViT (base) models from scratch with both MoCo and MAE paradigms, comparing learned slimmable training against standard (regular) training. All models are trained for 100 epochs on our curated RS dataset (see Section B in the appendix for an ablation on pretraining length). We evaluate both training paradigms across two downstream datasets, examining performance across the full range of computational budgets from 3 % to 100 % relative compute. Our results are shown in Figure 3. The results of the remaining datasets are provided in the appendix in Section F.

Slimmability improvements for MoCo but not for MAE
 MoCo-based learned slimmable training consistently outperforms regular training at low computational budgets while maintaining equivalent or superior performance at higher scales across all four tasks. For example, on m-eurosat (Figure 3a), slimmable MoCo shows marginal advantages at low scales that widen at intermediate budgets and full scale. On the challenging multi-label m-bigearthnet task (Figure 3b), both trained MoCo models converge to similar performance at full scale, with slimmable training converging noticeably faster. This consistent pattern demonstrates that explicit multi-scale optimization in MoCo-based training successfully structures representations to be more robust under width reduction without compromising maximum model capacity. In contrast to MoCo, learned slimmable training on MAEs shows no improvement compared to regular training. Rather, the opposite is the case: For m-eurosat (Figure 3a), the regular MAE outperforms the learned slimmable MAE across nearly all scales. The same is true for m-bigearthnet (Figure 3b), where the learned slimmable MAE even exhibits degradation when larger scales are applied. These

results suggests that MAE’s reconstruction objective interacts differently with multi-scale training depending on task complexity and label structure.

Contrastive learning advantages on multi-label tasks. Across both training paradigms, MoCo-based models substantially outperform MAE-based models specifically on m-bigearthnet, the only multi-label task in our evaluation suite. In contrast, on the single-label m-eurosat, MAE matches or exceeds MoCo’s performance. This indicates that contrastive learning’s instance discrimination objective may be more appropriate for multi-label classification, where models need to activate several independent semantic categories at once. On the other hand, the reconstruction objective of MAEs suffices for simpler single-label discrimination.

4.3. Why are some RS FMs more slimmable than others?

Feature correlation reveals distinct architectural scaling strategies. In Figure 4 we analyze mean feature correlations across scales, revealing fundamentally distinct scaling behaviors. DOFA (large) (Figure 4a) exhibits organized correlation of features at small scales before decreasing to near-independence at full scale, yet demonstrates monotonic performance improvement. This suggests that additional uncorrelated dimensions contribute useful orthogonal information. TerraMind-1.0 (large) (Figure 4b) shows slow monotonic correlation decrease, consistent with strong initial performance at low scales but diminishing marginal gains. This indicates that core discriminative features are efficiently encoded in early dimensions. Prithvi-EO-2.0 (600M) (Figure 4c) exhibits non-monotonic U-shaped patterns, with correlations decreasing to minima at intermediate scales before rebounding at full scale. This suggests that task-relevant information is already well-represented in compact subsets. These patterns indicate that strong correlation at smaller scales reflects effective feature concentration (beneficial for slimmability), whereas the benefit of extra capacity hinges on whether expanded dimensions introduce complementary (DOFA) or redundant (Prithvi) information. We provide additional experiments with more datasets and models in Section G in the appendix.

Explained variance analysis reveals scale-dependent feature reorganization. In Figure 5, we analyze representational anisotropy across scales. At scale 0.33 (Figure 5a), DOFA (large) exhibits pronounced anisotropy (first principal component (PC1) capturing >50 % variance) with rapid exponential decay, while Prithvi-EO-2.0 (600M) shows more isotropic representations (~30 %) with slower decay. This relationship reverses at full scale (Figure 5c): Prithvi becomes highly anisotropic (44.8 %) while DOFA balances (23 %). TerraMind-1.0 (large) maintains stable intermediate anisotropy (~34 %) across all scales.

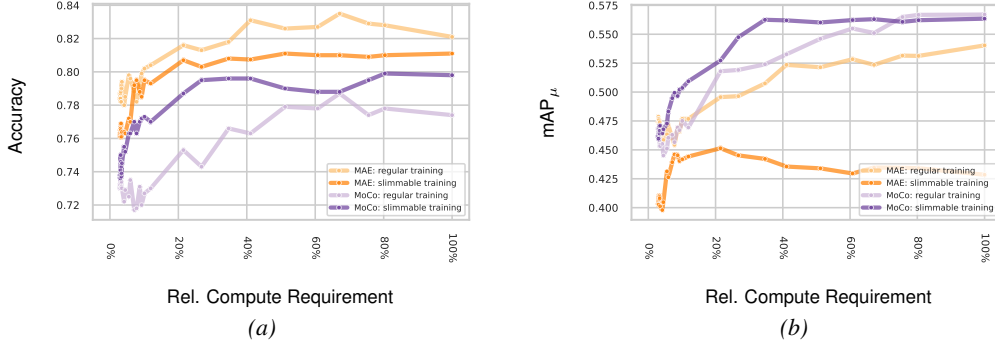


Figure 3. k-NN classification performance with respect to their relative compute requirements of a MAE-based and a MoCo-based trained model from scratch, each once with and once without slimmable training on: a) m-eurosat; and b) m-bigearthnet

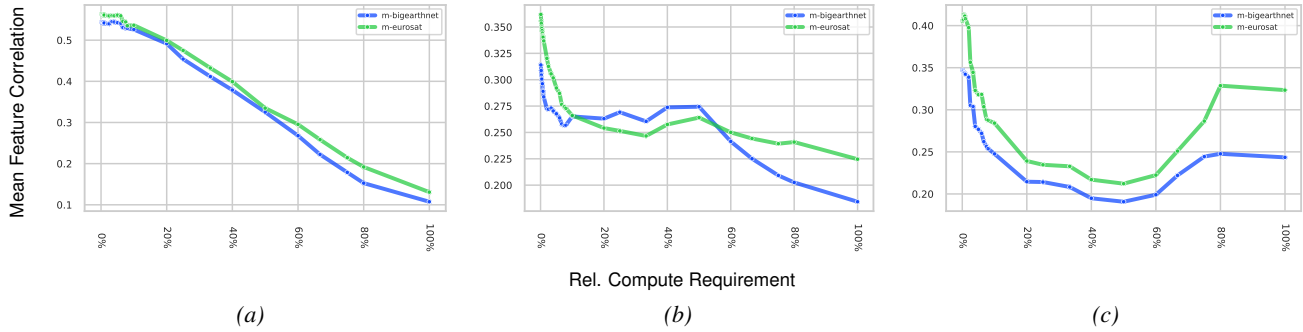


Figure 4. Mean Feature Correlation of the test split of m-eurosat and m-bigearthnet from the geobench benchmark collection with respect to their relative compute requirements on pretrained RS FMs: a) DOFA (large); b) TerraMind-1.0 (large); and c) Prithvi-EO-2.0 (600M).

When plotted in log-log space, all EVR curves exhibit approximately linear decay, indicating power-law behavior characterized by two parameters: intercept (initial variance concentration) and slope (decay rate). We summarize each profile as a single slope value, analyzed across scales in Figure 6. The slope analysis exposes distinct scaling behaviors: DOFA (large) shows monotonic slope increase from ~ -3.0 to -1.0 , indicating progressively distributed variance consistent with multi-modal training requiring diverse encodings. Prithvi-EO-2.0 (600M) exhibits non-monotonic U-shaped trajectories (slopes from -1.86 through maxima at 25–50 %, returning to -1.61), suggesting temporal training induces scale-dependent reorganization where intermediate capacities develop distributed representations before reconsolidating. TerraMind-1.0 (large) maintains stable slopes, reflecting land cover pretraining emphasizing scale-consistent features. Importantly, all models converge to steep slopes at very small scales ($< 5\%$), indicating that minimal-capacity models universally concentrate variance regardless of architecture. This reveals that training objectives primarily shape information distribution beyond minimal representations. Further results on additional models, datasets, and effective dimension analysis are provided in the appendix in Sections E and H.

5. Discussion

Our findings show that overparameterization in RS FMs enables substantial post-hoc slimming, a property absent in CV FMs. The sevenfold improvement in compression tolerance has immediate practical implications: practitioners can deploy existing RS FMs at drastically reduced computational budgets through simple uniform width reduction, without requiring sophisticated compression techniques.

Three key trends emerge with direct practical relevance. First, the systematic non-monotonic performance peaks observed across all datasets indicate that full-scale deployment is often suboptimal. Instead, intermediate scales often achieve superior accuracy through implicit regularization, offering up to $12\times$ speedups with performance improvements rather than degradation (as observed with Prithvi-EO-2.0 on m-brick-kiln). Second, the interaction between pretraining objective and task structure proves critical: MoCo-based slimmable training consistently improves low-scale performance, while MAE-based approaches excel on single-label tasks but cause severe degradation on multi-label scene classification. These results demonstrate that redundancy can be structured more consistently through learned slimmability, though effectiveness depends on the

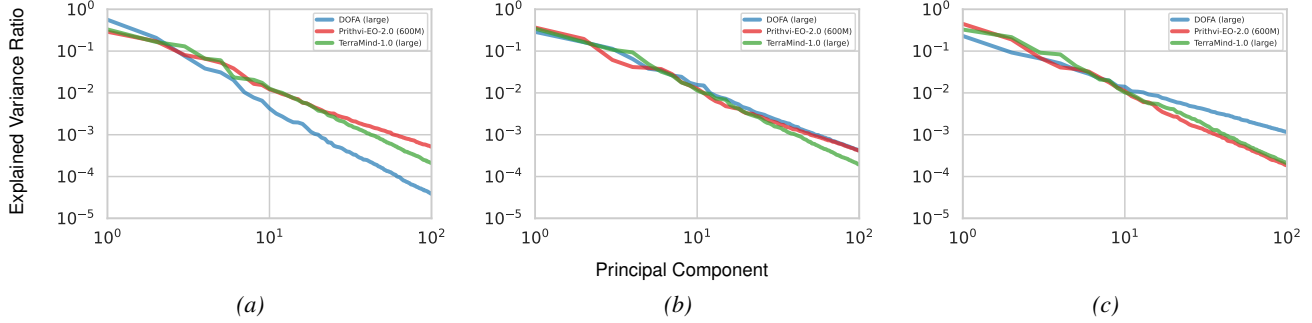


Figure 5. EVR with respect to the singular value rank index for three RS FMs on m-eurosat from the geobench benchmark collection at three relative compute requirements: a) 0.33; b) 0.67; and c) 1.0.

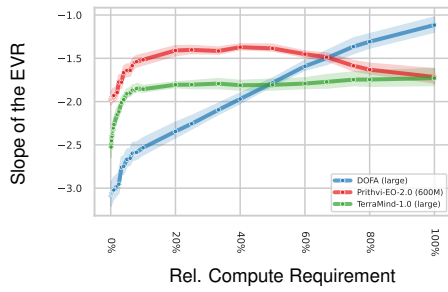


Figure 6. Log-Log-Slopes of the EVR with relative compute requirements for three different RS FMs averaged across four RS classifications datasets.

pretraining paradigm (e.g., reconstruction objectives interact poorly with multi-scale optimization when applied naively). Third, our geometric analysis reveals distinct scaling strategies tied to training objectives: Prithvi’s temporal pretraining induces non-monotonic U-shaped correlations, DOFA’s multi-modal approach produces monotonic variance ratios, while TerraMind maintains scale-invariant structure.

These insights enable a paradigm shift for the deployment of RS FM in which computational resources become a continuous optimization variable. Practitioners can select computational budgets based on predictable task-dependent behavior. For model development, we suggest prioritizing contrastive learning-based objectives with explicit slimmable training for the highest deployment flexibility, while the naive application of current slimmable methods on MAE-based training requires task-appropriate downstream tuning.

6. Conclusion and Future Work

We have presented the first systematic study of slimmability in RS FMs, demonstrating through an analysis of six state-of-the-art models across four downstream tasks that RS FMs retain over 70 % relative accuracy at 1 % compute, which results in a sevenfold improvement over CV FMs. Through explained variance and correlation analyses, we

established that this exceptional slimmability stems from highly redundant feature encodings rather than sparse hierarchical representations, providing mechanistic insights into how domain-specific data characteristics shape model scaling behaviors. Thus, we confirm our hypothesis that RS FMs enter an overparameterized regime at substantially smaller scales than CV models, in which additional capacity predominantly induces redundant representations rather than qualitatively new abstractions.

For practitioners deploying RS FMs under computational constraints, we recommend: i) evaluate uniform width reduction before complex pruning methods, as post-hoc slimming to 5–20 % compute often maintains >80 % accuracy; ii) scale computational budgets with task complexity: binary tasks tolerate <1 % compute while multi-label tasks require 10–20 %; iii) incorporate learned slimmability when training new RS FMs to maximize deployment flexibility; and iv) consider intermediate-scale deployment as it often achieves superior performance through implicit regularization. Future work should develop slimmable training techniques designed for MAE’s reconstruction objective, investigate modality-specific compression tolerances, and explore non-uniform slimming strategies that preserve critical architectural components while enabling greater compression.

Impact Statement

This paper presents work whose goal is to advance the field of Machine Learning. There are many potential societal consequences of our work, none which we feel must be specifically highlighted here.

References

Bastani, F., Wolters, P., Gupta, R., Ferdinando, J., and Kembhavi, A. Satlaspretrain: A large-scale dataset for remote sensing image understanding. In *Int. Conf. Comput. Vis.*, pp. 16772–16782, October 2023.

Bi, H., Feng, Y., Tong, B., Wang, M., Yu, H., Mao, Y., Chang, H., Diao, W., Wang, P., Yu, Y., Peng, H., Zhang, Y., Fu, K., and Sun, X. Ringmoe: Mixture-of-modality-experts multi-modal foundation models for universal remote sensing image interpretation. *arXiv preprint arXiv:2504.03166*, 2025.

Burgert, T., Stoll, O., Rota, P., and Demir, B. Imagenet-trained CNNs are not biased towards texture: Revisiting feature reliance through controlled suppression. In *Adv. Neural Inform. Process. Syst.*, volume 38, 2025.

Cao, Y.-H., Sun, P., and Zhou, S. Three guidelines you should know for universally slimmable self-supervised learning. In *IEEE Conf. Comput. Vis. Pattern Recog.*, pp. 15742–15751, June 2023.

Cong, Y., Khanna, S., Meng, C., Liu, P., Rozi, E., He, Y., Burke, M., Lobell, D., and Ermon, S. Satmae: Pre-training transformers for temporal and multi-spectral satellite imagery. In *Adv. Neural Inform. Process. Syst.*, volume 35, pp. 197–211, 2022.

Doimo, D., Glielmo, A., Goldt, S., and Laio, A. Redundant representations help generalization in wide neural networks. In *Adv. Neural Inform. Process. Syst.*, volume 35, pp. 19659–19672, 2022.

Francis, A. and Czerkawski, M. Major tom: Expandable datasets for earth observation. In *IEEE Int. Geosci. Remote Sens. Symp.*, pp. 2935–2940, 2024.

Guo, X., Lao, J., Dang, B., Zhang, Y., Yu, L., Ru, L., Zhong, L., Huang, Z., Wu, K., Hu, D., et al. Skysense: A multi-modal remote sensing foundation model towards universal interpretation for earth observation imagery. In *IEEE Conf. Comput. Vis. Pattern Recog.*, pp. 27672–27683, 2024.

Hackel, L., Burgert, T., and Demir, B. Csmoe: An efficient remote sensing foundation model with soft mixture-of-experts. *arXiv preprint arXiv:2509.14104*, 2025.

Hinton, G., Vinyals, O., and Dean, J. Distilling the knowledge in a neural network. *arXiv preprint arXiv:1503.02531*, 2015.

Hu, H., Wang, P., Bi, H., Tong, B., Wang, Z., Diao, W., Chang, H., Feng, Y., Zhang, Z., Wang, Y., et al. RS-vHeat: heat conduction guided efficient remote sensing foundation model. In *Int. Conf. Comput. Vis.*, pp. 9876–9887, 2025.

Jacob, B., Kligys, S., Chen, B., Zhu, M., Tang, M., Howard, A., Adam, H., and Kalenichenko, D. Quantization and training of neural networks for efficient integer-arithmetic-only inference. In *IEEE Conf. Comput. Vis. Pattern Recog.*, pp. 2704–2713, 2018.

Jakubik, J., Roy, S., Phillips, C. E., Fraccaro, P., Godwin, D., Zadrozny, B., Szwarcman, D., Gomes, C., Nyirjesy, G., Edwards, B., Kimura, D., Simumba, N., Chu, L., Mukkavilli, S. K., Lambhate, D., Das, K., Bangalore, R., Oliveira, D., Muszynski, M., Ankur, K., Ramasubramanian, M., Gurung, I., Khallaghi, S., Li, H. S., Cecil, M., Ahmadi, M., Kordi, F., Alemohammad, H., Maskey, M., Ganti, R., Weldemariam, K., and Ramachandran, R. Foundation models for generalist geospatial artificial intelligence. *arXiv preprint arxiv:2310.18660*, 2023.

Jakubik, J., Yang, F., Blumenstiel, B., Scheurer, E., Sedona, R., Maurogiovanni, S., Bosmans, J., Dionelis, N., Marsocci, V., Kopp, N., et al. Terramind: Large-scale generative multimodality for earth observation. In *Int. Conf. Comput. Vis.*, 2025.

Jiao, L., Huang, Z., Lu, X., Liu, X., Yang, Y., Zhao, J., Zhang, J., Hou, B., Yang, S., Liu, F., et al. Brain-inspired remote sensing foundation models and open problems: A comprehensive survey. *IEEE J. Sel. Topics Appl. Earth Observ. Remote Sens.*, 16:10084–10120, 2023.

Jing, L., Vincent, P., LeCun, Y., and Tian, Y. Understanding dimensional collapse in contrastive self-supervised learning. In *Int. Conf. Learn. Represent.*, 2022.

Lacoste, A., Lehmann, N., Rodriguez, P., Sherwin, E., Kerner, H., Lütjens, B., Irvin, J., Dao, D., Alemohammad, H., Drouin, A., et al. Geo-bench: Toward foundation models for earth monitoring. In *Adv. Neural Inform. Process. Syst.*, volume 36, pp. 51080–51093, 2023.

Li, C., Wang, G., Wang, B., Liang, X., Li, Z., and Chang, X. Dynamic slimmable network. In *IEEE Conf. Comput. Vis. Pattern Recog.*, pp. 8607–8617, 2021.

Li, H., Kadav, A., Durdanovic, I., Samet, H., and Graf, H. P. Pruning filters for efficient convnets. In *Int. Conf. Learn. Represent.*, 2017.

Liu, Z., Li, J., Shen, Z., Huang, G., Yan, S., and Zhang, C. Learning efficient convolutional networks through network slimming. In *Int. Conf. Comput. Vis.*, pp. 2736–2744, 2017.

Lu, S., Guo, J., Zimmer-Dauphinee, J. R., Nieusma, J. M., Wang, X., vanValkenburgh, P., Wernke, S. A., and Huo, Y. Vision foundation models in remote sensing: A survey. *IEEE Int. Geosci. Remote Sens. Mag.*, pp. 2–27, 2025.

Maktav, D., Erbek, F., and Jürgens, C. Remote sensing of urban areas. *T & F Int. J. Remote Sens.*, 26(4):655–659, 2005.

Omia, E., Bae, H., Park, E., Kim, M. S., Baek, I., Kabenge, I., and Cho, B.-K. Remote sensing in field crop monitoring: A comprehensive review of sensor systems, data

analyses and recent advances. *MDPI Remote Sens.*, 15(2):354, 2023.

Radford, A., Kim, J. W., Hallacy, C., Ramesh, A., Goh, G., Agarwal, S., Sastry, G., Askell, A., Mishkin, P., Clark, J., et al. Learning transferable visual models from natural language supervision. In *Int. Conf. Mach. Learn.*, pp. 8748–8763. PMLR, 2021.

Reed, C. J., Gupta, R., Li, S., Brockman, S., Funk, C., Clipp, B., Keutzer, K., Candido, S., Uyttendaele, M., and Darrell, T. Scale-mae: A scale-aware masked autoencoder for multiscale geospatial representation learning. In *Int. Conf. Comput. Vis.*, pp. 4088–4099, 2023.

Russakovsky, O., Deng, J., Su, H., Krause, J., Satheesh, S., Ma, S., Huang, Z., Karpathy, A., Khosla, A., Bernstein, M., Berg, A. C., and Fei-Fei, L. Imagenet large scale visual recognition challenge. *Int. J. Comput. Vis.*, 115(3):211–252, 2015.

Szwarcman, D., Roy, S., Fraccaro, P., Gíslason, P. E., Blumenstiel, B., Ghosal, R., de Oliveira, P. H., de Sousa Almeida, J. L., Sedona, R., Kang, Y., Chakraborty, S., Wang, S., Kumar, A., Truong, M., Godwin, D., Lee, H., Hsu, C.-Y., Akbari Asanjan, A., Mujeci, B., Keenan, T., Arévol, P., Li, W., Alemohammad, H., Olofsson, P., Hain, C., Kennedy, R., Zadrozny, B., Cavallaro, G., Watson, C., Maskey, M., Ramachandran, R., and Bernabe Moreno, J. Prithvi-eo-2.0: A versatile multi-temporal foundation model for earth observation applications. *arXiv preprint arXiv:2412.02732*, 2024.

Tian, Y., Krishnan, D., and Isola, P. Contrastive multiview coding. In *Eur. Conf. Comput. Vis.*, pp. 776–794. Springer, 2020.

Wang, Y., Braham, N. A. A., Xiong, Z., Liu, C., Albrecht, C. M., and Zhu, X. X. Ssl4eo-s12: A large-scale multimodal, multitemporal dataset for self-supervised learning in earth observation. *IEEE Int. Geosci. Remote Sens. Mag.*, 11(3):98–106, 2023.

Xiao, A., Xuan, W., Wang, J., Huang, J., Tao, D., Lu, S., and Yokoya, N. Foundation models for remote sensing and earth observation: A survey. *IEEE Int. Geosci. Remote Sens. Mag.*, pp. 2–29, 2025.

Xiong, Z., Wang, Y., Zhang, F., Stewart, A. J., Hanna, J., Borth, D., Papoutsis, I., Saux, B. L., Camps-Valls, G., and Zhu, X. X. Neural plasticity-inspired foundation model for observing the Earth crossing modalities. *arXiv preprint arXiv:2403.15356*, 2024.

Yamazaki, F. and Matsuoka, M. Remote sensing technologies in post-disaster damage assessment. *Journal of Earthquake and Tsunami*, 1(03):193–210, 2007.

Yang, J., Gong, P., Fu, R., Zhang, M., Chen, J., Liang, S., Xu, B., Shi, J., and Dickinson, R. The role of satellite remote sensing in climate change studies. *Nature climate change*, 3(10):875–883, 2013.

Yu, J. and Huang, T. S. Universally slimmable networks and improved training techniques. In *Int. Conf. Comput. Vis.*, pp. 1803–1811, 2019.

Yu, J., Yang, L., Xu, N., Yang, J., and Huang, T. Slimmable neural networks. In *Int. Conf. Learn. Represent.*, 2019.

Zhang, H., Li, F., Liu, S., Zhang, L., Su, H., Zhu, J., Ni, L., and Shum, H.-Y. DINO: DETR with improved denoising anchor boxes for end-to-end object detection. In *Int. Conf. Learn. Represent.*, 2023.

Zhao, S., Zhu, L., Wang, X., and Yang, Y. Slimmable networks for contrastive self-supervised learning. *Int. J. Comput. Vis.*, 133(3):1222–1237, 2025.

How Much of a Model Do We Need? Redundancy and Slimmability in Remote Sensing Foundation Models

Appendix

Appendix Overview

- [A](#) Slimmability of Different Layer Types
- [B](#) Details on Training from Scratch
- [C](#) Details on the Evaluation Protocol
- [D](#) Linear Evaluation
- [E](#) Effective Dimensionality Analysis
- [F](#) Additional Experiments on Learned vs Post-Hoc Slimmability
- [G](#) Feature Correlation at different Model Scales
- [H](#) Additional Experiments on Explained Variance

A. Slimmability of Different Layer Types

To understand the computational contributions of different architectural components, we compare three slimming strategies: i) slimming only FFN layers while keeping MHSA at full width; ii) slimming only MHSA layers while keeping FFN at full width; and iii) slimming both layer types simultaneously. The results of these experiments are shown in Figure 7.

As one can see from the figure, our analysis reveals that MHSA and FFN layers contribute asymmetrically to both computational cost and representational capacity. Models slimmed exclusively through MHSA width reduction (blue lines) cannot achieve relative compute requirements below 60 %, as the fixed-width FFN layers dominate the computational budget. Moreover, MHSA-only slimming exhibits steeper performance degradation relative to compute reduction compared to FFN-only approaches, suggesting that attention mechanisms encode more task-critical information per compute. In contrast, FFN-only slimming (orange lines) enables compression down to 35 % relative compute while maintaining more gradual performance decay. This indicates that FFN layers contribute disproportionately to FLOPs but contain more redundant parameters that can be removed with minimal performance impact.

However, simultaneous slimming of both layer types (green lines) proves superior across all evaluated models, enabling compression to 1 % relative compute while exhibiting the most gradual performance degradation curves. This synergistic effect suggests that maintaining architectural balance, where MHSA and FFN widths scale proportionally, preserves the learned feature processing pipeline more effectively than asymmetric compression. The ability to slim both components simultaneously also provides access to the full computational range, from 1–100 % of original FLOPs, enabling fine-grained deployment optimization. From a

practical deployment perspective, practitioners should prioritize simultaneous slimming of both layer types to maximize compression ratios while maintaining performance, rather than attempting to preserve specific architectural components at full capacity.

B. Details on Training from Scratch

To investigate learned slimmability (Contribution C2), we train both MoCo and MAE architectures with and without slimmable training on a curated RS dataset. We use the dataset from [Hackel et al. \(2025\)](#), which applies entropy-maximizing stratified sampling to Major Tom Core (MTC) ([Francis & Czerkawski, 2024](#)) based on Köppen-Geiger climate zones and ESA WorldCover classes, yielding approximately 100 spatially diverse samples per joined stratum and a total of ~ 1 M training patches at 120×120 pixels. All models use a ViT-Tiny backbone with 10 input channels (10 m and 20 m Sentinel-2 bands) and image size 224×224 pixels.

Training Protocol. Standard (non-slimmable) training is conducted for 300 epochs with batch size of 384 per GPU and AdamW optimizer ($\beta_1 = 0.9$, $\beta_2 = 0.95$, weight decay 0.05). The learning rate follows a linear warmup for 1% of total steps, followed by cosine annealing from base learning rate $lr_{base} \times \frac{batch\ size}{256}$ to $\frac{lr_{base}}{100}$, where $lr_{base} = 10^{-4}$. For MoCo, we use momentum encoder update with cosine schedule from 0.996 to 1.0 over 10 epochs, projection head dimension 128, and normalized temperature-scaled cross entropy (NT-Xent) loss with memory bank size 4096. For MAE, we use mask ratio 0.75, decoder dimension 512, decoder depth 1, and 16 decoder heads with mean squared error (MSE) reconstruction loss. All pretraining experiments were run on 4 NVIDIA A100-80GB GPUs or 4 NVIDIA H200-141GB GPUs.

Slimmable Pretraining. Learned slimmable training extends the standard protocol to 800 epochs to account for the increased optimization difficulty. During each training step, we perform manual optimization with multiple forward-backward passes: i) the full network at scale $s = 1.0$ with standard task loss; ii) the minimal network at scale s_{min} with task loss plus knowledge distillation from the full network; and iii) three randomly sampled intermediate scales with the same combined loss. The minimal scale s_{min} linearly decreases from 0.5 to 0.01 over the first 50 % of training to encourage robust feature learning across scales following ([Zhao et al., 2025](#)). Knowledge distillation uses temperature-

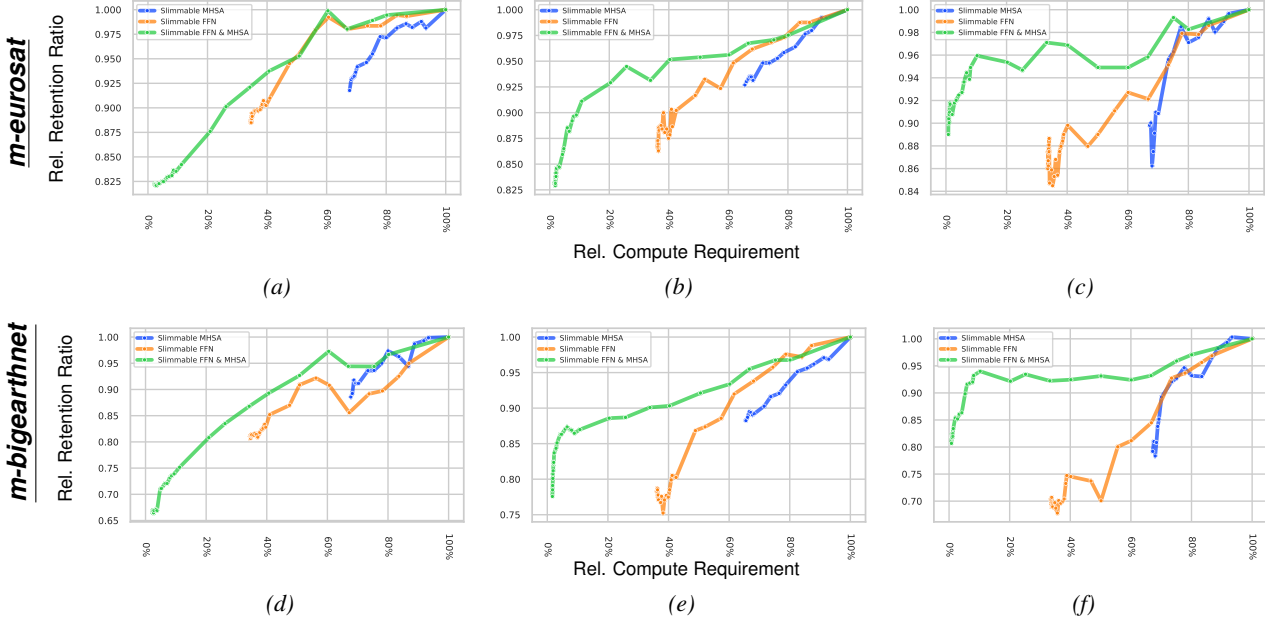


Figure 7. k-NN relative retention rate with respect to their relative compute requirements for slimming only the FFN layer, only the MHSA layer, or both layers simultaneously of: a) DOFA (large); b) TerraMind-1.0 (large); and c) Prithvi-EO-2.0 (600M) on m-eurosat; and e) DOFA (large); f) TerraMind-1.0 (large); and g) Prithvi-EO-2.0 (600M) on m-bigearthnet.

scaled KL divergence with $T = 1.0$ between features passed through a two-layer MLP distillation head ($d \rightarrow 2d \rightarrow d$ with GELU activation). This multi-scale training encourages weight sharing and robustness across the entire range of network widths.

Evaluation. We evaluate all resulting models at multiple intermediate checkpoints (every 50 epochs for the first 300 epochs, then every 100 epochs) on the m-eurosat dataset from the geobench benchmark collections using our k-NN evaluation protocol. The results of this evaluation can be seen in Figure 8. As one can see from the figures, for regular training the accuracy increases of the full network increases with additional training for both MAE and MoCo architectures (Figure 8a and 8c) although only small or marginal improvements can be seen after 100 epochs. For smaller scales (with respective lower compute requirements), the accuracy is not monotonously increasing with longer training.

For slimmable training, in the case of MAE (Figure 8b) the accuracy raises across all scales for the first 200 epochs, then sharply declines by almost 20 % and then slowly increases over the following 600 epochs but never fully recovers. The slimmably trained MoCo model decreases accuracy for higher compute requirements (larger than 20 %) but increases for smaller ones. Overall the accuracy equalizes for this model across all compute requirements with longer training.

C. Details on the Evaluation Protocol

C.1. Scale Evaluation

During k-NN and linear evaluation, we evaluate each model on 31 scales: {0.001, 0.002, 0.0025, 0.00333, 0.004, 0.005, 0.006, 0.00667, 0.0075, 0.008, 0.01, 0.02, 0.025, 0.0333, 0.04, 0.05, 0.06, 0.0667, 0.075, 0.08, 0.1, 0.2, 0.25, 0.333, 0.4, 0.5, 0.6, 0.667, 0.75, 0.8, 1.0}. The reduced dimensions $d'_k = \lfloor s \cdot d_k \rfloor$ and $d'_h = \lfloor s \cdot d_h \rfloor$ are at minimum 1, meaning multiple scales can result in the same reduced dimension for small values of s .

C.2. Feature Extraction and Downstream Tasks

Feature Extraction. For all models and scales, we extract features from the penultimate layer (before the final classification head or pooling operation) on both training and test sets of each downstream dataset. Features are saved as NumPy arrays along with their corresponding labels to enable efficient repeated evaluation without recomputing features.

k-NN Evaluation. We use $k = 5$ neighbors and temperature parameter $t = 0.9$ for the weighted KNN classifier. Classification is performed using cosine similarity between test features and the training feature bank. For the binary dataset (m-brick-kiln) and multi-class datasets (m-eurosat, m-so2sat), we compute macro-averaged accuracy. For the multi-label m-bigearthnet dataset, we report micro-averaged mAP_μ .

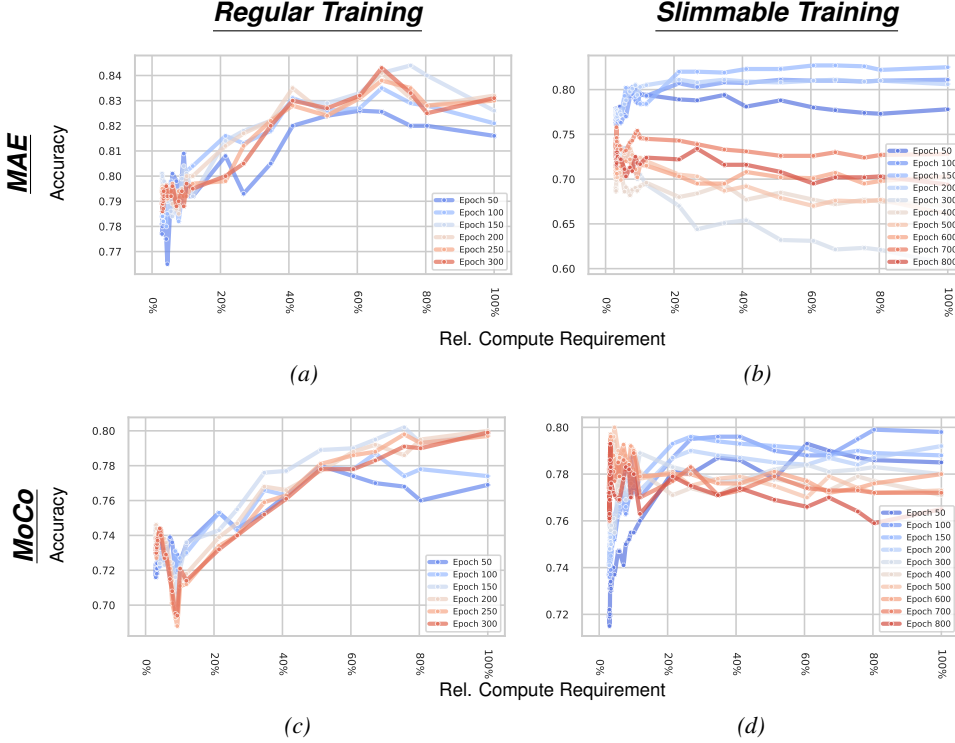


Figure 8. k-NN classification performance regards to their relative compute requirements of a MAE-based and a MoCo-based trained model from scratch, each once with and once without slimmable training on m-eurosat for different training durations: a) regular MAE; b) slimmable MAE; c) regular MoCo; d) slimmable MoCo.

Linear Probing. Linear classifiers are trained for 50 epochs using AdamW optimizer with learning rate 0.05, batch size 64, and no weight decay. For multi-class tasks, we use cross-entropy loss; for multi-label m-bigearthnet, we use binary cross-entropy with logits. We report the same metrics as for k-NN evaluation.

Experimental Repeatability. Each experiment is performed five times with different random seeds, and averaged results are reported to account for variability in both feature extraction (at different scales) and downstream evaluation. All downstream evaluations were run on single NVIDIA A40-48GB GPUs.

D. Linear Evaluation

We evaluate DOFA (large), TerraMind-1.0 (large), and Prithvi-EO-2.0 (600M) on m-eurosat and m-bigearthnet both as k-NN and linear probing using the evaluation protocol described in Section C.2. The results of this evaluation are shown in Figure 9. As one can see from the figure, for all evaluations except for m-bigearthnet on Prithvi-EO-2.0 (600M) the linear classification accuracy is higher for larger scales (with larger compute requirements). Still, for m-bigearthnet on Prithvi-EO-2.0 (600M) the linear classification accuracy is higher for $0.0667 \leq s \leq 0.8$. Addi-

tionally, for most cases there is a specific size \tilde{s} where the k-NN accuracy is higher if $s < \tilde{s}$ and lower if $s > \tilde{s}$. Only for m-eurosat on Terramind-1.0 (large) the linear classification accuracy is higher than the k-NN accuracy for all sizes and for m-bigearthnet on Prithvi-EO-2.0 (600M) there are three sizes (5 %, 6 %, and 100 %) that do not follow this monotony. To summarize, in general pretrained models benefit from linear probing only for larger sizes whereas k-NN evaluation is stronger for models which are more rigorously slimmed. However, the size \tilde{s} where smaller sizes benefit from k-NN evaluation is not consistent for a specific model or dataset.

E. Effective Dimensionality Analysis

In Figure 10, we analyze the relationship between effective dimensionality and relative retention rate across selected RS FMs. Our analysis reveals fundamentally different feature space organization strategies. DOFA models (Figure 10a and 10b) exhibit pathological concentration of task-relevant information in ultra-low-dimensional subspaces, achieving effective dimensions below 5 at minimal scales (0.1 %) while retaining 53–87 % of full-scale performance. However, reaching full performance requires expanding to up to 313 effective dimensions for only 13–47 % additional gain, resulting in up to 52× dimensionality increases for

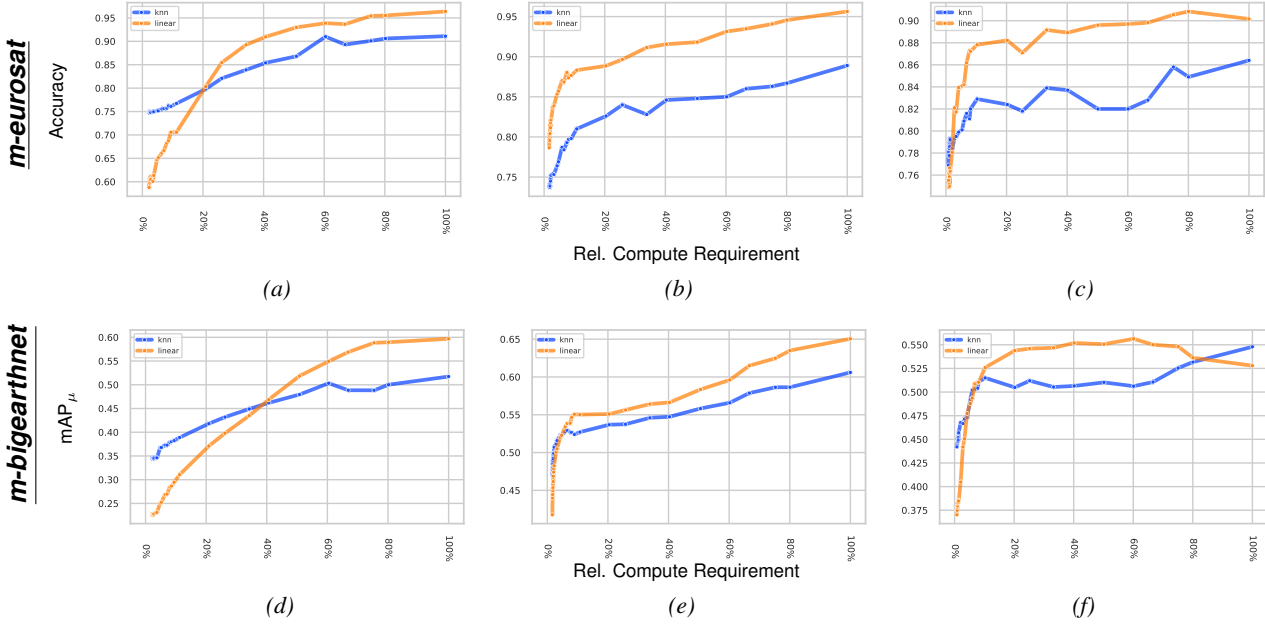


Figure 9. k-NN and linear classification accuracy with respect to their relative compute requirements of: a) DOFA (large); b) TerraMind-1.0 (large); and c) Prithvi-EO-2.0 (600M) on m-eurosat; and e) DOFA (large); f) TerraMind-1.0 (large); and g) Prithvi-EO-2.0 (600M) on m-bigearthnet.

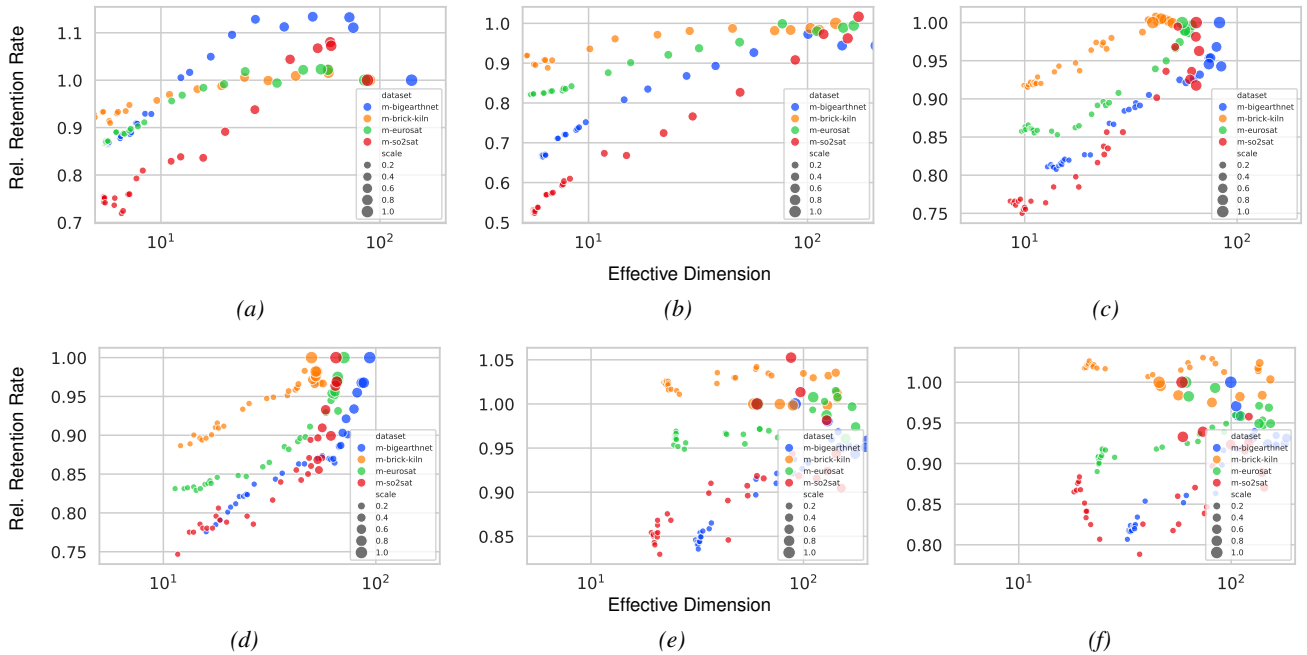


Figure 10. Effective Dimension of the test split of four classification datasets from the geobench benchmark collection with respect to their relative compute requirements on pretrained RS FMs: a) DOFA (base); b) DOFA (large); c) TerraMind-1.0 (base); d) TerraMind-1.0 (large); e) Prithvi-EO-2.0 (300M); and f) Prithvi-EO-2.0 (600M) on m-bigearthnet;

marginal improvements. This shows severe overdimensionality where 300+ additional dimensions minimally contribute to discrimination. In contrast to that, Prithvi-EO-2.0 (600M) (Figure 10f) distributes task-relevant information across moderately-dimensional subspaces, maintaining at least 81 % performance retention with maximally 33 effective dimensions at minimal scales. Although this represents 6.5 \times higher dimensionality than DOFA (large) at comparable retention rates, Prithvi-EO-2.0 exhibits distinctive non-monotonic trajectories: effective dimensions increase from 33 at minimal scales through peaks of 183 at intermediate scales before decreasing to 99 at full scale. This U-shaped pattern indicates deliberate dimensionality reduction and feature consolidation in the final capacity regime, mirroring the non-monotonic slope behavior observed in the EVR analysis (Figure 6).

The contrasting strategies reveal fundamental architectural differences: Prithvi’s 3–6 \times higher minimal effective dimensionality (18–33 vs. 4.6–6.1) enables superior performance retention (81–102 % vs. 53–87 %), demonstrating that distributed feature encoding across moderately-dimensional subspaces enables robust slimmability without catastrophic degradation. Conversely, DOFA’s ultra-compact concentration necessitates massive dimensionality expansion for modest gains, providing quantitative evidence that well-organized feature spaces require moderate intrinsic dimensionality even at minimal scales. Notably, Prithvi’s non-monotonic effective dimension trajectory and the similar pattern in its EVR slope evolution may also indicate incomplete convergence during pretraining, suggesting that additional training could potentially stabilize its feature space organization and yield more consistent scaling behavior.

F. Additional Experiments on Learned vs Post-Hoc Slimmability

We provide additional results for the remaining two datasets (m-brick-kiln and m-so2sat) to complement the main analysis of learned versus post-hoc slimmability. These additional evaluations further validate the training paradigm-dependent patterns observed on m-eurosat and m-bigearthnet, while revealing nuanced task-complexity effects.

Binary and fine-grained classification results. For the binary m-brick-kiln dataset (Figure 11a), slimmable MoCo achieves marginal improvements at low computational budgets (0.842 vs 0.838 accuracy at 3 % compute) and peaks at 0.896 at 41 % compute compared to 0.893 for regular training at 51 % compute. Both trained models converge near 0.89 at moderate scales, confirming that learned slimmability maintains performance parity at full capacity while improving low-scale robustness. For the learned slimmable MAE, the pattern shows disadvantages at very low scales (0.869 vs 0.878 at 3 %) that inverse at intermediate budgets

(0.916 vs 0.879 at 21 %), though regular MAE ultimately dominates at maximum scale (0.940 vs 0.925).

The fine-grained m-so2sat dataset (Figure 11b) reveals more pronounced differences. Slimmable MoCo substantially outperforms regular training, achieving 0.296 accuracy at 3 % compute versus 0.280 and reaching a peak of 0.334 at 8 % compute, thereby surpassing regular MoCo’s maximum of 0.314 at 51 % compute by 6.4 % relative accuracy while requiring less than 20 % of the compute. Remarkably, the learned slimmable MAE completely reverses the degradation pattern observed on m-bigearthnet, dominating across all evaluated scales with 0.340 accuracy at 3 % compute versus 0.292 for regular MAE, maintaining this advantage through full scale (0.386 vs 0.365).

Task complexity determines MAE slimmability benefits.

These additional results establish a clear relationship between task complexity and MAE slimmability performance. Learned slimmable MAE exhibits severe degradation on the complex multi-label m-bigearthnet task, marginal disadvantages on the binary m-brick-kiln task, underperformance on the intermediate m-eurosat task, but strong advantages on the fine-grained single-label m-so2sat task. This progression suggests that MAE’s reconstruction objective benefits from learned slimmability specifically for intermediate-complexity single-label tasks, while multi-scale optimization interferes with the mask-reconstruction representations needed for either very simple binary discrimination or complex multi-label semantic tasks. In contrast, MoCo’s instance discrimination objective demonstrates consistent slimmability improvements across all task complexities, confirming that contrastive learning and slimmable training can be successfully combined to develop FMs for flexible deployment across diverse downstream applications.

G. Feature Correlation at different Model Scales

We provide an extended feature correlation analysis across all six RS FMs and four datasets in Figure 12. The analysis reveals that distinct correlation shapes remain consistent across both model sizes and datasets, indicating that these patterns are fundamental characteristics of training paradigms rather than task-specific adaptations.

The DOFA models (Figures 12a and 12b) exhibit a characteristic correlation shape across all datasets: highly organized feature correlations at small scales transitioning to near-independence at full scale. Notably, the DOFA (base) model shows less correlated features at small scales but more at large scales compared to the DOFA (large), resulting in a less steep transition slope. Despite this difference in slope steepness, both models share the same fundamental correlation shape that remains consistent across binary (m-brick-

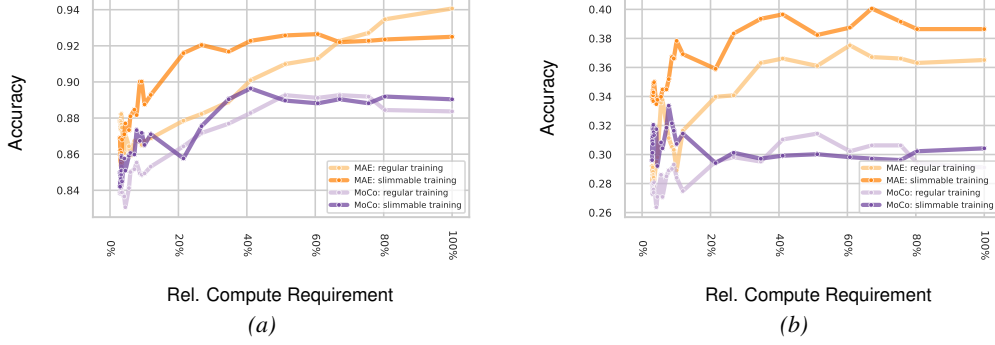


Figure 11. k-NN classification performance with respect to their relative compute requirements of a MAE-based and a MoCo-based trained model from scratch, each once with and once without slimmable training on: a) m-brick-kiln; and b) m-so2sat

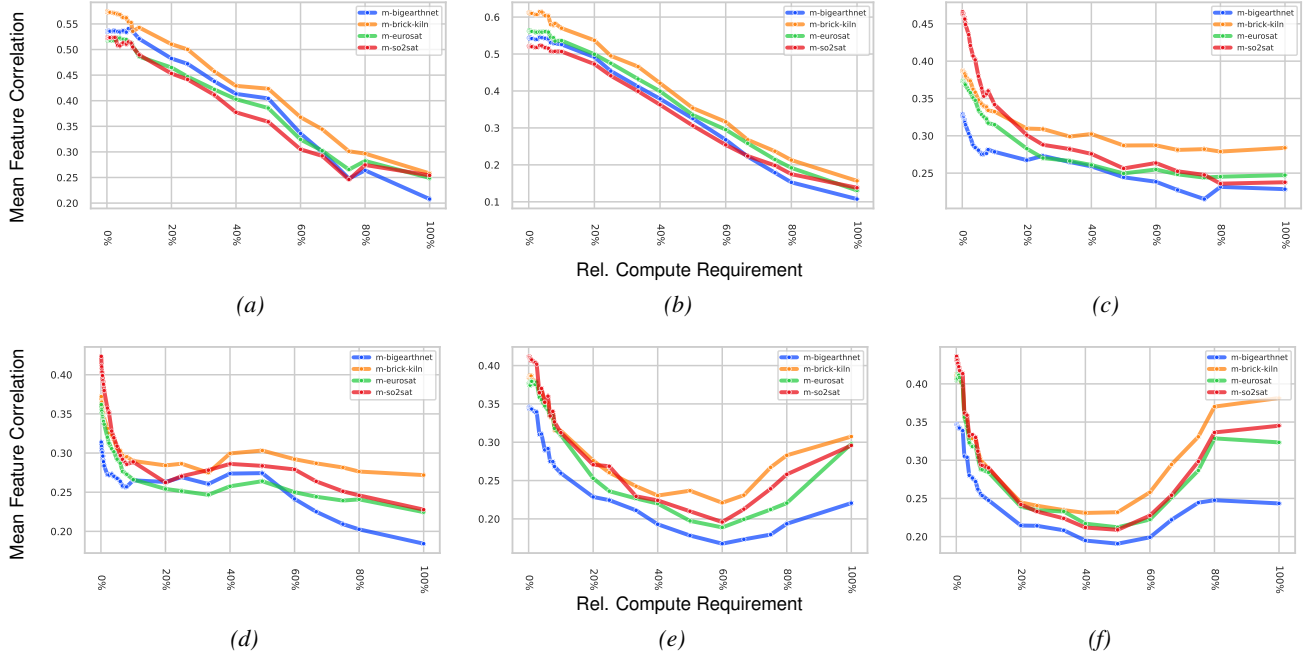


Figure 12. Mean Feature Correlation of the test split of four classification datasets from the geobench benchmark collection with respect to their relative compute requirements on pretrained RS FMs: a) DOFA (base); b) DOFA (large); c) TerraMind-1.0 (base); d) TerraMind-1.0 (large); e) Prithvi-EO-2.0 (300M); and f) Prithvi-EO-2.0 (600M).

Figure partially overlaps with Figure 4, but we visualize all data for ease of comparison.

kiln), intermediate (m-eurosat), fine-grained (m-so2sat), and multi-label (m-bigearthnet) tasks. This consistent pattern, combined with monotonic performance improvement across scales, confirms that additional uncorrelated dimensions at full scale contribute useful orthogonal information despite the correlation collapse.

The TerraMind-1.0 models (Figures 12c and 12d) demonstrate identical correlation shapes across both base and large sizes, characterized by smooth and mostly monotonic decrease from moderate to low correlations. The TerraMind-1.0 (base) model maintains higher correlation values across all scales compared to TerraMind-1.0 (large), and exhibits a slightly smoother slope, but the fundamental shape remains unchanged. This shape consistency across model sizes and datasets indicates that TerraMind-1.0’s training paradigm induces a stable feature organization strategy where core discriminative features are efficiently encoded in early dimensions, with larger models simply distributing this information more independently.

Prithvi-EO-2.0 models (Figures 12e and 12f) exhibit the distinctive non-monotonic U-shaped correlation pattern across both Prithvi-EO-2.0 (300M) and Prithvi-EO-2.0 (600M) and all datasets. While the Prithvi-EO-2.0 (300M) model shows a less pronounced rebound at large scales, not reaching as high correlations as the Prithvi-EO-2.0 (600M) variant, the U-shaped character remains clearly visible. This consistent U-shape, characterized by moderate initial correlations, drops at low-to-intermediate scales, and subsequent rebounds at full scale, suggests that Prithvi’s temporal training objective induces systematic scale-dependent feature reorganization regardless of model capacity or downstream task complexity.

The remarkable consistency of these correlation shapes across model sizes and datasets establishes that each model family develops a characteristic feature organization strategy determined by its training paradigm: DOFA’s multi-modal training produces high-to-low correlation transitions, TerraMind-1.0’s land cover focus maintains smooth monotonic decrease, and Prithvi-EO-2.0’s temporal modeling induces non-monotonic U-shaped patterns.

H. Additional Experiments on Explained Variance

We provide an extended EVR analysis across all six RS FMs and four datasets in Figure 13. The extended analysis confirms the log-log slope patterns observed in Figure 6 while revealing model family-specific consistency across datasets and scales. Both Prithvi-EO-2.0 and both TerraMind-1.0 models exhibit remarkable internal consistency: within each model family, both sizes demonstrate nearly identical EVR decay patterns across all datasets and

scales. This consistency indicates that these models’ variance distribution strategies are determined primarily by their training objectives rather than their parameter count. The Prithvi-EO-2.0 models maintain their characteristic non-monotonic pattern (becoming more isotropic at intermediate scales before reconsolidating at full scale) across all datasets, while the TerraMind-1.0 models preserve stable intermediate anisotropy regardless of whether evaluated on binary, multi-class, or multi-label tasks. In contrast, the DOFA models exhibit systematic scale-dependent behavior that varies between base and large variants but remains consistent across datasets. Both DOFA models demonstrate steeper slopes (more concentrated variance) at smaller scales and shallower slopes (more distributed variance) at larger scales across all four datasets, with the base model maintaining systematically steeper slopes than the large variant at equivalent relative compute budgets. This pattern confirms the observation that DOFA’s multi-modal training drives monotonic variance redistribution as capacity increases, with larger models distributing variance more evenly. The consistency of this pattern across binary (m-brick-kiln), intermediate (m-eurosat), fine-grained (m-so2sat), and multi-label (m-bigearthnet) tasks demonstrates that DOFA’s scaling strategy is an architectural property rather than a task-specific adaptation.

These findings reinforce the conclusion that training objectives fundamentally determine how models organize information across scales, with this organization remaining stable across diverse downstream task requirements.

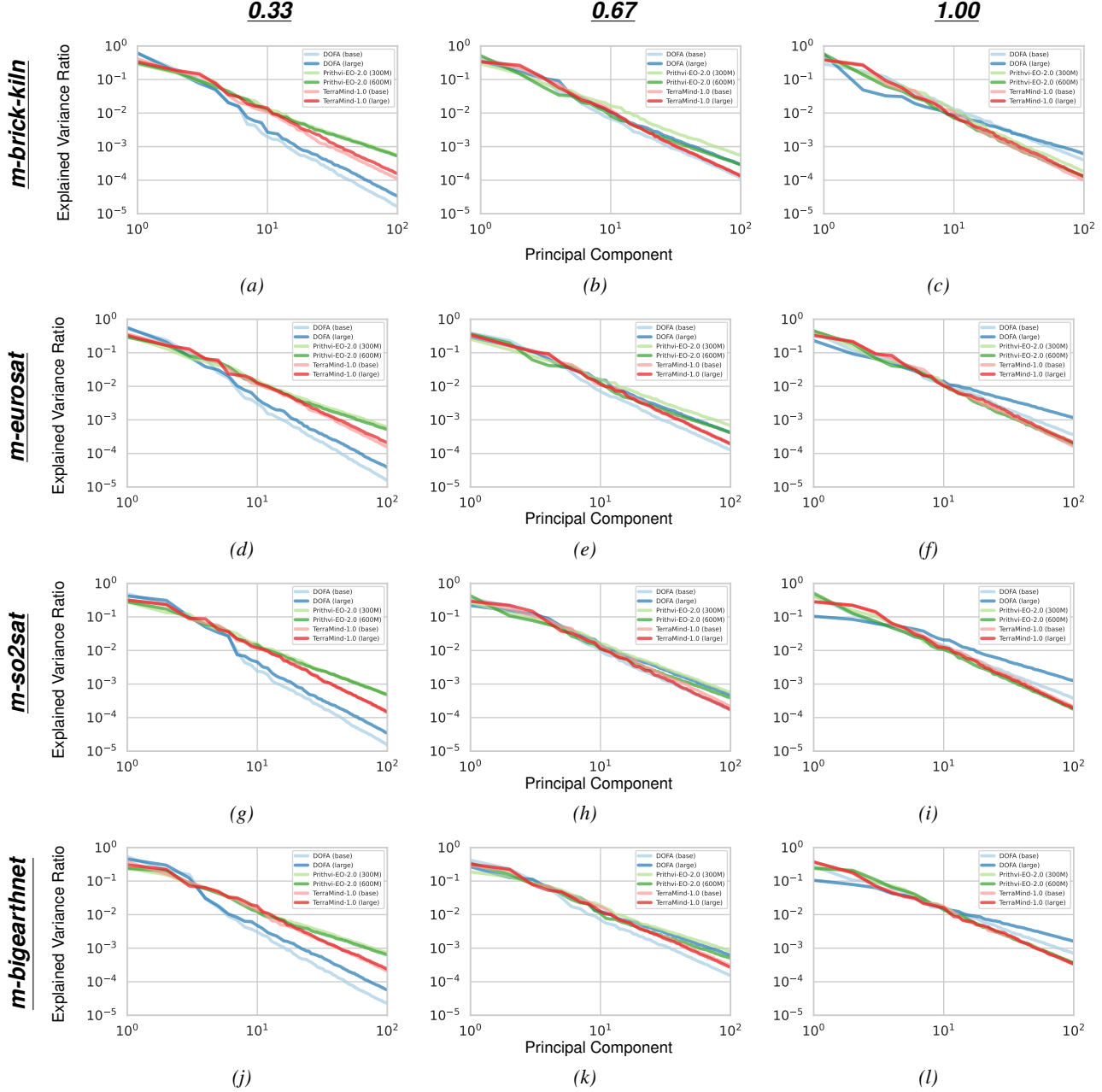


Figure 13. EVR with respect to the singular value rank index for six RS FMs on four classification datasets from the geobench benchmark collection at three relative compute requirements: 0.33; 0.67; and 1.0. Figures (d), (e), and (f) with Figure 5.